

Accepted Manuscript

Photocatalytic Reduction of CO₂ by Cu_xO Nanocluster loaded SrTiO₃ Nanorod Thin Film

Shusaku Shoji, Ge Yin, Masami Nishikawa, Daiki Atarashi, Etsuo Sakai, Masahiro Miyauchi

PII: S0009-2614(16)30457-2

DOI: <http://dx.doi.org/10.1016/j.cplett.2016.06.062>

Reference: CPLETT 33971

To appear in: *Chemical Physics Letters*

Received Date: 22 May 2016

Accepted Date: 22 June 2016

Please cite this article as: S. Shoji, G. Yin, M. Nishikawa, D. Atarashi, E. Sakai, M. Miyauchi, Photocatalytic Reduction of CO₂ by Cu_xO Nanocluster loaded SrTiO₃ Nanorod Thin Film, *Chemical Physics Letters* (2016), doi: <http://dx.doi.org/10.1016/j.cplett.2016.06.062>

This is a PDF file of an unedited manuscript that has been accepted for publication. As a service to our customers we are providing this early version of the manuscript. The manuscript will undergo copyediting, typesetting, and review of the resulting proof before it is published in its final form. Please note that during the production process errors may be discovered which could affect the content, and all legal disclaimers that apply to the journal pertain.



Photocatalytic Reduction of CO₂ by Cu_xO Nanocluster loaded SrTiO₃
Nanorod Thin Film

Shusaku Shoji,[†] Ge Yin,[†] Masami Nishikawa,[‡] Daiki Atarashi,[†] Etsuo Sakai,[†] Masahiro
Miyauchi^{†*}

[†] Department of Materials Science and Engineering, School of Materials and Chemical
Technology, Tokyo Institute of Technology, 2-12-1 Ookayama, Meguro-ku, Tokyo 152-8552,
Japan

[‡] Department of Materials Science and Technology, Nagaoka University of Technology, 1603-1,
Kamitomioka-machi, Nagaoka, Niigata 940-2188, Japan

*Corresponding author.

Prof. Masahiro Miyauchi

Email: mmiyauchi@ceram.titech.ac.jp

Tel:+81-3-5734-2527

[Insert Running title of <72 characters]

Abstract

Photocatalytic carbon dioxide (CO₂) conversion into carbon monoxide (CO) using H₂O as an electron donor was achieved by the strontium titanate (SrTiO₃; STO) nanorod thin films loaded with amorphous copper oxide (Cu_xO) nanoclusters. The loading of the Cu_xO-cocatalysts onto STO nanorods clearly improved the photocatalytic activity compared to bare STO nanorods. The Cu_xO-cocatalysts are composed of abundant and non-toxic elements, and can be loaded by using a simple and economical method. Our findings demonstrate that Cu_xO nanoclusters function as a general cocatalyst and can be used in combination with various semiconductors to construct low-cost and efficient photocatalytic CO₂ reduction systems.

Keywords: photocatalyst, nanorods, cocatalyst, Cu_xO nanocluster, Impregnation method, CO₂ reduction, ubiquitous elements, ESR analysis, Isotope labeling analysis.

[Insert Running title of <72 characters]

Introduction

Photocatalytic carbon dioxide reduction, in which CO₂ is converted into organic compounds, such as methane, methanol, formic acid, and formaldehyde, has the potential to greatly contribute to reducing global warming and fossil fuel dependence.[1,2] In a photocatalytic CO₂ reduction system, photoexcited electrons in the conduction band reduce CO₂, while photogenerated holes in the valence band oxidize the electron donor. Since Halmann[3] reported that p-type gallium phosphide functions as a photocatalyst for CO₂ reduction into methanol, formic acid, or formaldehyde, various semiconductor photocatalysts have been studied, including TiO₂, ZnO, CdS, GaP, SiC,[4] Zn-doped Ga₂O₃,[5] and SrTiO₃. [6] In artificial photosynthesis systems designed for the reduction of CO₂ for solar fuel production, water molecules should ideally serve as the electron donor, similar to photosystems I and II in natural plants. Further, the CO₂ reduction reaction competes with the reduction of protons to produce molecular hydrogen. However, because the redox potential of H⁺/H₂ (-0.41 V vs NHE at pH 7) is lower than that of CO/CO₂ (-0.53 V vs NHE at pH 7)[2], the proton reduction reaction is thermodynamically favored. Therefore, increasing the selectivity of CO₂ reduction products over hydrogen generation is critical for the development of efficient photocatalytic systems for CO₂ reduction.

One approach for improving the products selectivity of semiconductor photocatalysts is the loading of cocatalysts to drive oxidation or reduction selectivity. For example, Sato *et al.*[7,8] efficiently reduced CO₂ using a combination of ruthenium complex cocatalyst and either N-doped Ta₂O₅, GaP or InP semiconductors. In addition to complex cocatalysts, metal nanoparticles also exhibit high selectivity for CO₂ reduction, as demonstrated for silver (Ag)-loaded ALa₄Ti₄O₁₅ (A= Ca, Sr, or Ba) and Ag cluster-loaded Ga₂O₃. [9] Au-Cu alloy nanoparticles were also reported to function as a cocatalyst when loaded onto SrTiO₃/TiO₂ photocatalyst.[10] In contrast to noble metal organic complexes and particles, copper and copper oxide are ubiquitous in the environment and are nontoxic. Further, copper compounds have balanced chemisorption-

[Insert Running title of <72 characters]

desorption properties for CO₂ and CO, [11,12] and therefore have high CO₂ reduction activity[13,14] and high selectivity of products, such as carbon monoxide and formic acid (HCOOH).[15,16] In addition to the requirement for high CO₂/CO chemisorption-desorption, cocatalysts must accumulate photogenerated electrons at specific reaction sites to drive efficient CO₂ photoreduction, as CO₂ reduction proceeds via a multi-electron process. For example, two electrons are required for CO and HCOOH production, and six electrons are needed for CH₃OH generation. Recently, our group reported that a copper oxide nanocluster cocatalyst drives the multi-electron reduction of both oxygen to produce hydrogen peroxide[17,18] and CO₂ to generate CO.[19] For copper oxide cocatalysts to drive CO₂ photoreduction, light-harvesting semiconductors with a high conduction band, such as niobate nanosheets, are required, as the photoreduction of CO₂ requires excited electrons with a higher potential energy than that needed for hydrogen production.[19] During the CO₂ reduction reaction, copper oxide consists of Cu(I) and Cu(II) valence states and is designated as Cu_xO (x=1 or 2).

Herein, we examined the potential of strontium titanate (SrTiO₃: STO) to function as a light harvester with loading of Cu_xO cocatalysts, as the STO has high chemical stability and sufficient negative conduction band for CO₂ reduction.[20] In addition, compared to reported light harvesters, including niobate materials, STO has a relatively narrow band gap and unique crystal structure. As the band gap of STO (3.2 eV) is narrower than that of niobate (3.56 eV), STO is expected more effectively utilize solar energy than niobate. Further, the crystal phase of STO is a perovskite structure (ABO₃), which enables doping and the maintenance of charge balance by co-doping into A and B sites.[21,22] In the present research, we used STO nanorod thin films[23] as a UV-light harvester due to its high crystallinity and increased surface area for the loading -of Cu_xO cocatalyst. The photocatalytic CO₂ reduction activity of Cu_xO cocatalyst loaded STO nanorod (Cu_xO-STO) thin films was evaluated under UV-light irradiation in the present study. In addition, excited species in Cu_xO-STO were investigated by electron spin resonance (ESR)

[Insert Running title of <72 characters]

analysis to examine the charge separation process. Further, isotope labeling experiments with $^{13}\text{CO}_2$ and H_2^{18}O isotopes were used to confirm that the generated CO originated from CO_2 and that the electron donor was water.

Materials and Methods

Synthesis of STO nanorod thin films

STO nanorod thin films were synthesized by the annealing of strontium ion-exchanged titanate nanotube thin films.[23] Titanate nanotube thin film was prepared by the hydrothermal treatment of titanium (Ti) foil ($2 \times 2 \times 0.1$ cm, Nilaco Co.).[24] Briefly, Ti foil was immersed in 30 mL of 10 M aqueous NaOH solution and allowed to react in a 100-mL Teflon-lined autoclave at 413 K for 3 h. After cooling to room temperature, the titanate nanotube thin film was washed with distilled water and immersed in a 0.1 M HNO_3 aqueous solution for 1 day to protonate the interlayer of the titanate nanotube thin film. The protonated film was immersed in a saturated aqueous solution of 2 M strontium acetate for 1 day to exchange the protons in the interlayer of the titanate nanotubes with strontium ions (Sr^{2+}). The ion-exchanged sample was then annealed at 923 K for 2 h in air. The samples were washed with a 0.1 M HNO_3 aqueous solution to remove strontium carbonate from the nanotube thin film surface. For the measurement of optical absorption of STO nanorod excluding the signal from metal Ti substrate, powder form of STO nanorod was also synthesized with the same manner to the fabrication of STO nanorod thin film. Titanate nanotube powder was prepared by the hydrothermal treatment of TiO_2 (P-25) powder in 10 M NaOH aqueous solution for 1 day.

Loading of Cu_xO nanocluster cocatalyst onto STO nanorod thin films

[Insert Running title of <72 characters]

Cu_xO nanocluster cocatalyst was loaded onto the STO nanorod thin films using an impregnation method.[25] Briefly, the STO nanorod thin film was immersed into 60 mL of a CuCl₂ aqueous solution in a glass beaker. The Cu_xO nanoclusters were then loaded onto the STO films through initiation of a hydrolysis reaction in the aqueous medium at 363 K for 1 h. The fraction weight of Cu was set to be 0 to 0.005 wt% against H₂O. The synthesized Cu_xO-STO nanorod thin films were washed with distilled water and dried at 378 K in air. Cu_xO nanoclusters were also loaded onto the STO nanorod powder by the similar manner.

Characterization

Crystal structures of the obtained samples were determined by X-ray diffraction (XRD; Rigaku, SmartLab) using Cu- $k\alpha$ X-rays ($\lambda=1.5418 \text{ \AA}$). The incident angle was fixed at 1.2 degrees and the 2θ scan angle ranged from 5 to 60 degrees. The sample morphologies were observed by scanning electron microscopy (SEM; JSM-7500F, JEOL, Ltd.) and transmission electron microscopy (TEM; JEM-2010F, JEOL, Ltd.). Chemical compositions of the sample were investigated using an energy dispersive X-ray spectroscope (EDX: PHI5000) equipped with a TEM apparatus. The valence number of copper nanoclusters was determined by measuring electron spin resonance (ESR; EMX Plus, Bruker) under an N₂ atmosphere. The ESR results were recorded as differential spectra between the bare STO nanorod and Cu_xO-STO thin films. X-ray photoelectron spectroscopy (XPS; model ESCA-5500MT, Perkin Elmer Instruments, Japan) analysis was conducted to investigate the Cu-2p core level using standard Mg K α X-rays.

Photocatalytic CO₂ reduction

[Insert Running title of <72 characters]

The prepared Cu_xO -STO film was added to an electrolyte solution (20 mL) consisting of 0.5 M KHCO_3 and adjusted to $\text{pH}=12$ using aqueous NaOH , in a sealed quartz glass reactor (500 mL). To purge air in the reactor, CO_2 or Ar gasses were bubbled into the reactor through a Teflon tube at a flow rate of 100 mL/min for 30 min. Carbonic acid ions were formed in an aqueous media by the addition of KHCO_3 and bubbling of CO_2 . In the case of Ar bubbling conditions, 0.5 M KCl aqueous solution, which was adjusted to $\text{pH}= 12$, was used as the electrolyte. Products in the headspace of the reactor were evaluated using a gas chromatograph (flame ionization detector (FID)) equipped with a methanizer unit under UV light irradiation (Hg-Xe lamp, LA-410UV; Hayashi Watch Works, Ltd.). An isotope experiment was also conducted in a quartz glass cell ($1\times 1\times 5$ cm) to verify that the generated O_2 and CO originated from the photocatalytic reduction of CO_2 with water as an electron donor. A $0.5\times 2.0\times 0.1$ cm section of Cu_xO -STO film was immersed into a 0.5 M $\text{KH}^{13}\text{CO}_3$ (Isotec-Sigma-Aldrich) aqueous H_2^{18}O (Isotec-Sigma-Aldrich) solution in the quartz glass cell. The headspace and electrolyte were saturated with $^{13}\text{CO}_2$ (Isotec-Sigma-Aldrich) gas for 5 min bubbling, and the cell was then irradiated with UV light. Products in the headspace of the cell were evaluated by gas chromatography-mass spectrometry (GC-MS; Shimadzu). Before performing the photocatalytic CO_2 reduction measurements, samples were irradiated under UV light in air to remove surface organic contaminants.

Results and Discussion

Structural and morphological properties

Figure 1 shows the XRD patterns of the prepared Cu_xO -STO thin films. Hydrothermal treatment of Ti foil converted the polycrystalline metal titanium to a layered hydrogen titanate [Insert Running title of <72 characters]

crystal structure.[24] After the titanate film was immersed in a saturated aqueous solution of strontium acetate and annealed in air, the film adopted the perovskite structure of STO.

Annealing treatment on the Sr^{2+} ion-exchanged titanate nanotubes generated STO, as perovskite-type STO is composed of corner-sheared TiO_6 octahedrons, which have a similar lattice structure as the edges of titanate nanosheets.

We measured the optical absorption properties of Cu_xO -STO nanorod and STO nanorod powders, which were prepared by the same manner with the thin film fabrication, to exclude the optical signal from metal titanium substrate. The UV-Vis spectra recorded by a diffuse reflectance method are shown in our supporting information (Figure S1). The band-to-band transition of the STO nanorod started around 380 nm, and the absorption at 430 nm of Cu_xO -STO nanorod is attributable to interfacial charge transfer (IFCT).[26] The broad absorption around 580-800 nm is assigned to the d-d transition of the Cu(II) species.[27] The bandgap of the STO nanorod was estimated to be 3.2 eV, as calculated from the intersection of the plotted line of square root of absorption coefficient versus photon energy with the abscissa axis.

Figure 2 shows SEM and TEM images of the STO nanorod and Cu_xO -STO nanorod thin films. The SEM image revealed that the film surface was porous and numerous rods were uniformly covered on a titanium foil substrate. The TEM image revealed that amorphous nanoclusters of 2-3 nm in size were attached and highly dispersed on the STO nanorods. Energy dispersive X-ray (EDX) spectroscopy analysis was conducted at the point on an STO nanorod that was considered to be a Cu_xO nanocluster cocatalyst (Figure 2b). And as a result of the EDX spectrum, a signal corresponding to Cu was clearly observed at the position of small nanoclusters (Figure 2c). The EDX signal of molybdenum (Mo) was attributed to a contaminant from the sample grid holder.

[Insert Running title of <72 characters]

To determine the chemical state of the Cu_xO nanocluster cocatalyst and the behaviour of the photo-excited electrons, ESR was measured before and after UV irradiation of the Cu_xO -STO film (Figure 3). We also measured the ESR spectrum of bare STO nanorod thin film, and did not detect any obvious peaks corresponding to copper ions or any changes to the spectrum after UV irradiation. In contrast, the Cu_xO -STO film exhibited a broad ESR peak, which was assigned to Cu^{2+} species, around 345 mT under dark conditions, and this peak decreased in intensity after UV irradiation (Figure 3). As ESR detects unpaired electrons, the decrease of the Cu^{2+} peak under UV irradiation indicates that the valence number of the Cu^{2+} species, which contain nine electrons in the d-orbital, partially changed to Cu^+ , which is inactive for ESR. Thus, under UV-light irradiation, photo-excited electrons of STO were injected into the Cu_xO nanocluster cocatalyst. In the ESR analysis, trapped holes were not detected. It is assumed that the holes in the trapping site were inhomogeneous and that the ESR signal became broad due to its nanorod structure. We also measured XPS spectrum for the Cu_xO -STO film (supporting information, Figure S2). Two peaks of Cu-2p core level were observed, whereas these peaks were not appeared on the bare STO nanorod film. The peak at 933 eV corresponds to Cu $2p_{3/2}$, while that at 953 eV corresponds to Cu $2p_{1/2}$. [28] If the sample contained Cu^{2+} species, satellite peaks would be appeared at 942 and 962 eV. [29-31] However, these satellite peaks were not observed in our sample, thus the copper species mainly consist of Cu^{1+} species, resulting from the bombardment effect by X-ray irradiation under high vacuum. [17] Our previous X-ray absorption near edge structure (XANES) spectra revealed the as-prepared Cu_xO nanocluster mainly composed of Cu^{2+} species, [17] thus the Cu_xO nanoclusters in the present study also consist of amorphous CuO at the as-prepared condition.

[Insert Running title of <72 characters]

Photocatalytic CO₂ reduction

Figure 4 shows the time course of photocatalytic CO generation for bare STO and Cu_xO-STO film under UV irradiation with Ar or CO₂ bubbling conditions. The amount of Cu_xO in the film was optimized to be 0.0005 wt%, as described below. The CO generation rate was highest for Cu_xO-STO under CO₂ bubbling conditions and was markedly reduced under Ar bubbling conditions, whereas that of bare STO was limited under both CO₂ and Ar bubbling conditions. The small amount of CO production detected under Ar bubbling was attributed to the oxidation of organic contaminants adsorbed on the film surface, even though the surface of the samples was cleaned by pre-irradiation treatment in air. To prove the photocatalytic CO generation under CO₂ bubbling condition, we have conducted isotope trace experiment as described later. We also evaluated the hydrogen (H₂) production under UV irradiation (see our supporting information, Figure S3). Although small amount of H₂ was detected, main product by our photocatalyst was CO, indicating its high selectivity for CO₂ photoreduction. It is noteworthy that the loading of Cu_xO onto STO exhibited 20 % improvement of selectivity for CO₂ photoreduction.

Figure 5 shows the influence of the amount of loaded Cu_xO nanocluster cocatalyst on the photocatalytic CO generation activity of STO nanorod thin films. Based on the analysis, the optimum amount of Cu_xO for efficient CO production was determined to be 0.0005 wt% in the solution used for Cu_xO loading. Below optimum condition, the amount of Cu_xO is insufficient, while those are overloaded above optimum condition. The trend of photocatalytic activity versus the amount of Cu_xO nanoclusters will be explained in our discussion section below.

We next conducted isotope tracer analysis on the optimized Cu_xO-STO film (Figure 6). The peaks in the mass chromatography spectra at $m/z = 29$ and 36 were assigned to ¹³CO and ¹⁸O₂, respectively. These results confirmed that the CO generated by the Cu_xO-STO film originated
[Insert Running title of <72 characters]

from CO₂, and that O₂ molecules were produced through water oxidation. Similar to photosystems I and II in natural plants, our Cu_xO-STO film system generates fuel from stable molecules like CO₂ and water in an uphill reaction under photon irradiation.

Discussion on photocatalytic process

Here, we discuss the cocatalytic effect of the Cu_xO nanoclusters for CO₂ reduction. According to previous electrochemical studies, copper elements effectively promoted CO₂ electro-reduction under cathodic bias. For example, Kortlever *et al.* [32] reported that CO₂ reduction proceeded by two alternate pathways, one involving the generation of formate species and the other leading to the production of CO species, ultimately resulting in the formation of various final products, including methane and hydrocarbon. We monitored formic acid production in the electrolyte solution, and found that only a negligible amount of formic acid was produced. Further, no significant differences in formic acid production were detected between the CO₂ and Ar bubbling conditions. Azuma *et al.* [14] reported that copper catalyzed the reduction of CO₂ molecules to CO species rather than formate. This finding is consistent with our present results that the Cu_xO nanoclusters have high selectivity for CO generation and do not promote hydrogen or formate formation.

Next, we discuss the photoexcitation process of the Cu_xO-STO film. There are three expected excitation processes as follows,

1. interband transition in STO and electron injection from the conduction band of STO to Cu²⁺
2. d-d transition in Cu²⁺ species
3. interfacial charge transfer (IFCT) from the valence band of STO valence band to Cu²⁺ (Interfacial charge transfer [18])

[Insert Running title of <72 characters]

The bandgap of STO was 3.2 eV and its optical absorption was appeared under 380 nm as shown in our supporting information (Figure S1). On the other hand, the absorption of Cu^{2+} by d-d transition was appeared above 580 nm, while that by IFCT was appeared around 400 to 430 nm (Figure S1). We have investigated visible light activity under a Xe lamp with a UV cutoff filter, which could excite both d-d transition and IFCT. However, any CO was not produced under visible light irradiation. These results indicate that the d-d transition and IFCT do not contribute to the CO_2 photoreduction. Therefore, our photocatalytic CO_2 reduction is driven by the interband transition of STO and following electron injection from the conduction band of STO into Cu_xO clusters, which act as reactive sites for CO_2 reduction. Also, our ESR analysis under UV irradiation indicated that electrons are injected from the conduction band of STO into the Cu_xO nanoclusters.

Although the conduction band of STO is higher than the redox potential of CO_2/CO , the redox potential of Cu(II)/Cu(I) (+0.16 V vs NHE at pH 0)[25,33] is lower than that of CO_2/CO . Despite the lower redox potential of Cu(II)/Cu(I) , our experimental results revealed that CO_2 was reduced to CO by the UV irradiation of Cu_xO -STO film. The efficiency of the CO_2 photoreduction reaction is due to a negative shift of the Fermi level of the Cu_xO nanocluster resulting from the injection of excited electrons from the conduction band of STO. Therefore, the mixed valence states of the Cu species in Cu_xO was critical for the ability of this cocatalyst to promote CO_2 reduction. Yin *et al.*[19] reported that the initial chemical composition of Cu_xO clusters loaded onto niobate nanosheets was CuO, and that a proportion of the Cu(II) species in the clusters were converted to Cu(I) during the initial 3 h of UV-light irradiation. After 5 h of irradiation, Cu(II) and Cu(I) were balanced and CO_2 photoreduction was efficient and stable. As

[Insert Running title of <72 characters]

observed in Figure 5, the size or amount of the Cu_xO nanoclusters also influenced the upshift in the Cu_xO Fermi level following electron injection.

Conclusion

We have demonstrated the applicability of modifying SrTiO_3 with Cu_xO nanoclusters as a cocatalyst for CO_2 photoreduction. The Cu_xO -STO film exhibited high activity and selectivity for CO evolution under UV irradiation. The isotope tracer analysis confirmed that water served as an electron donor and that CO molecules were produced by the reduction of CO_2 under UV irradiation. Similar to photosystems in natural plants, fuel molecules were successfully generated by the Cu_xO -STO film from CO_2 and water in response to photon irradiation. The key underlying factors for the efficient multi-electron reduction of CO_2 by this system are the high conduction band of STO and the loading of highly dispersed Cu_xO clusters onto the STO surface. Further, as the Cu_xO is composed of non-toxic and abundant elements, it has the potential to be an effective cocatalyst onto various light-harvesting materials to achieve CO_2 photo-reduction.

Acknowledgements

This research was supported by a grant from the Advanced Catalytic Transformation Program for Carbon Utilization (ACT-C) of the Japan Science and Technology Agency (JST), and JSPS KAKENHI Grant Number 26410234. We thank Mr. K. Hori at the Center for Advanced Materials Analysis of the Tokyo Institute of Technology for helping with the TEM characterization. We also thank Mr. H. Hara at the Bruker Corporation for measuring ESR spectra.

[Insert Running title of <72 characters]

References Primary Sources**Secondary Sources****Uncategorized References**

- [1] J. Hansen, L. Nazarenko, R. Ruedy, M. Sato, J. Willis, A. Del Genio, D. Koch, A. Lacis, K. Lo, S. Menon, T. Novakov, J. Perlwitz, G. Russell, G.A. Schmidt, N. Tausnev, *Science* 308 (2005) 1431.
- [2] S.N. Habisreutinger, L. Schmidt-Mende, J.K. Stolarczyk, *Angewandte Chemie (International ed. in English)* 52 (2013) 7372.
- [3] M. Halmann, *Nature* 275 (1978) 115.
- [4] T. Inoue, A. Fujishima, S. Konishi, K. Honda, *Nature* 277 (1979) 637.
- [5] K. Teramura, Z. Wang, S. Hosokawa, Y. Sakata, T. Tanaka, *Chemistry (Weinheim an der Bergstrasse, Germany)* 20 (2014) 9906.
- [6] M. Halmann, M. Ulman, B. Aurian-Blajeni, *Solar Energy* 31 (1983) 429.
- [7] S. Sato, T. Arai, T. Morikawa, K. Uemura, T.M. Suzuki, H. Tanaka, T. Kajino, *Journal of the American Chemical Society* 133 (2011) 15240.
- [8] S. Sato, T. Morikawa, S. Saeki, T. Kajino, T. Motohiro, *Angewandte Chemie (International ed. in English)* 49 (2010) 5101.
- [9] M. Yamamoto, T. Yoshida, N. Yamamoto, T. Nomoto, Y. Yamamoto, S. Yagi, H. Yoshida, *Journal of Materials Chemistry A* 3 (2015) 16810.
- [10] Ş. Neaţu, J.A. Maciá-Agulló, P. Concepción, H. Garcia, *Journal of the American Chemical Society* 136 (2014) 15969.
- [11] R.G. Copperthwaite, P.R. Davies, M.A. Morris, M.W. Roberts, R.A. Ryder, *Catalysis Letters* 1 11.
- [12] K.P. Kuhl, T. Hatsukade, E.R. Cave, D.N. Abram, J. Kibsgaard, T.F. Jaramillo, *Journal of the American Chemical Society* 136 (2014) 14107.
- [13] Y. Hori, A. Murata, R. Takahashi, *Journal of the Chemical Society, Faraday Transactions 1: Physical Chemistry in Condensed Phases* 85 (1989) 2309.
- [14] M. Azuma, K. Hashimoto, M. Hiramoto, M. Watanabe, T. Sakata, *Journal of The Electrochemical Society* 137 (1990) 1772.
- [15] K. Hara, A. Kudo, T. Sakata, *Journal of Electroanalytical Chemistry* 391 (1995) 141.
- [16] R. Reske, H. Mistry, F. Behafarid, B. Roldan Cuenya, P. Strasser, *Journal of the American Chemical Society* 136 (2014) 6978.
- [17] X. Qiu, M. Miyauchi, K. Sunada, M. Minoshima, M. Liu, Y. Lu, D. Li, Y. Shimodaira, Y. Hosogi, Y. Kuroda, K. Hashimoto, *ACS Nano* 6 (2011) 1609.
- [18] M. Miyauchi, H. Irie, M. Liu, X. Qiu, H. Yu, K. Sunada, K. Hashimoto, *The journal of physical chemistry letters* 7 (2016) 75.
- [19] G. Yin, M. Nishikawa, Y. Nosaka, N. Srinivasan, D. Atarashi, E. Sakai, M. Miyauchi, *ACS nano* 9 (2015) 2111.
- [20] D.E. Scaife, *Solar Energy* 25 (1980) 41.
- [21] M. Miyauchi, M. Takashio, H. Tobimatsu, *Langmuir* 20 (2004) 232.

[Insert Running title of <72 characters]

- [22] R. Konta, T. Ishii, H. Kato, A. Kudo, *The Journal of Physical Chemistry B* 108 (2004) 8992.
- [23] M. Miyauchi, *The Journal of Physical Chemistry C* 111 (2007) 12440.
- [24] M. Miyauchi, H. Tokudome, Y. Toda, T. Kamiya, H. Hosono, *Applied Physics Letters* 89 (2006) 043114.
- [25] M. Liu, X. Qiu, M. Miyauchi, K. Hashimoto, *Chemistry of Materials* 23 (2011) 5282.
- [26] X. Qiu, M. Miyauchi, K. Sunada, M. Minoshima, M. Liu, Y. Lu, D. Li, Y. Shimodaira, Y. Hosogi, Y. Kuroda, K. Hashimoto, *ACS nano* 6 (2012) 1609.
- [27] N.L. Dias Filho, *Microchimica Acta* 130 233.
- [28] V. Hayez, A. Franquet, A. Hubin, H. Terryn, *Surf Interface Anal* 36 (2004) 876.
- [29] J.C. Otamiri, S.L.T. Andersson, A. Andersson, *Applied Catalysis* 65 (1990) 159.
- [30] M.C. Biesinger, B.P. Payne, A.P. Grosvenor, L.W.M. Lau, A.R. Gerson, R.S.C. Smart, *Applied Surface Science* 257 (2011) 2717.
- [31] S. Poulston, P.M. Parlett, P. Stone, M. Bowker, *Surf Interface Anal* 24 (1996) 811.
- [32] R. Kortlever, J. Shen, K.J.P. Schouten, F. Calle-Vallejo, M.T.M. Koper, *The Journal of Physical Chemistry Letters* 6 (2015) 4073.
- [33] H. Irie, S. Miura, K. Kamiya, K. Hashimoto, *Chemical Physics Letters* 457 (2008) 202.

Figure Captions

Figure. 1 XRD patterns of Ti foil (a), titanate nanotube thin film (b), and STO nanorod thin film (c). Triangles, circles, and diamonds indicate metal titanium, layered hydrogen titanate, and strontium titanate crystals, respectively.

Figure. 2 Structural analyses of Cu_xO -STO film. SEM image of the surface of STO nanorod thin film observed on the surface (a). TEM image of a Cu_xO nanocluster cocatalyst-loaded STO nanorod (b). Panel (c) shows the EDX spectrum at the point marked by a circle in the TEM image (b).

Figure. 3 ESR spectra of the Cu_xO -STO film under dark and UV-irradiated conditions.

[Insert Running title of <72 characters]

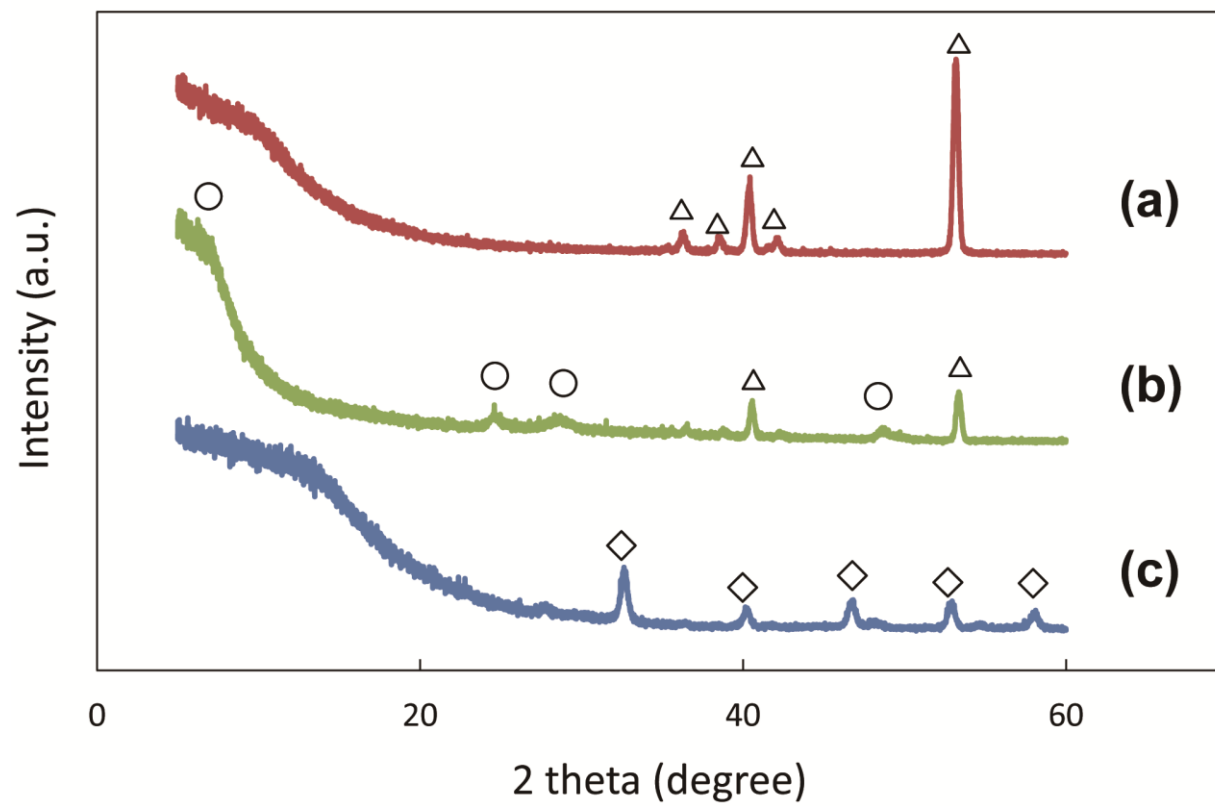
Figure. 4 Time course of photocatalytic carbon monoxide (CO) generation by Cu_xO -STO and bare STO nanorod thin films.

Figure. 5 Relationship between photocatalytic CO generation rate and concentration of Cu^{2+} solution used for Cu_xO loading.

Figure. 6 Mass chromatography spectra of ^{13}CO ($m/z=29$) and $^{18}\text{O}_2$ ($m/z=36$) generated during the photocatalytic reduction of $^{13}\text{CO}_2$ by the optimized Cu_xO -STO film in the presence of H_2^{18}O .

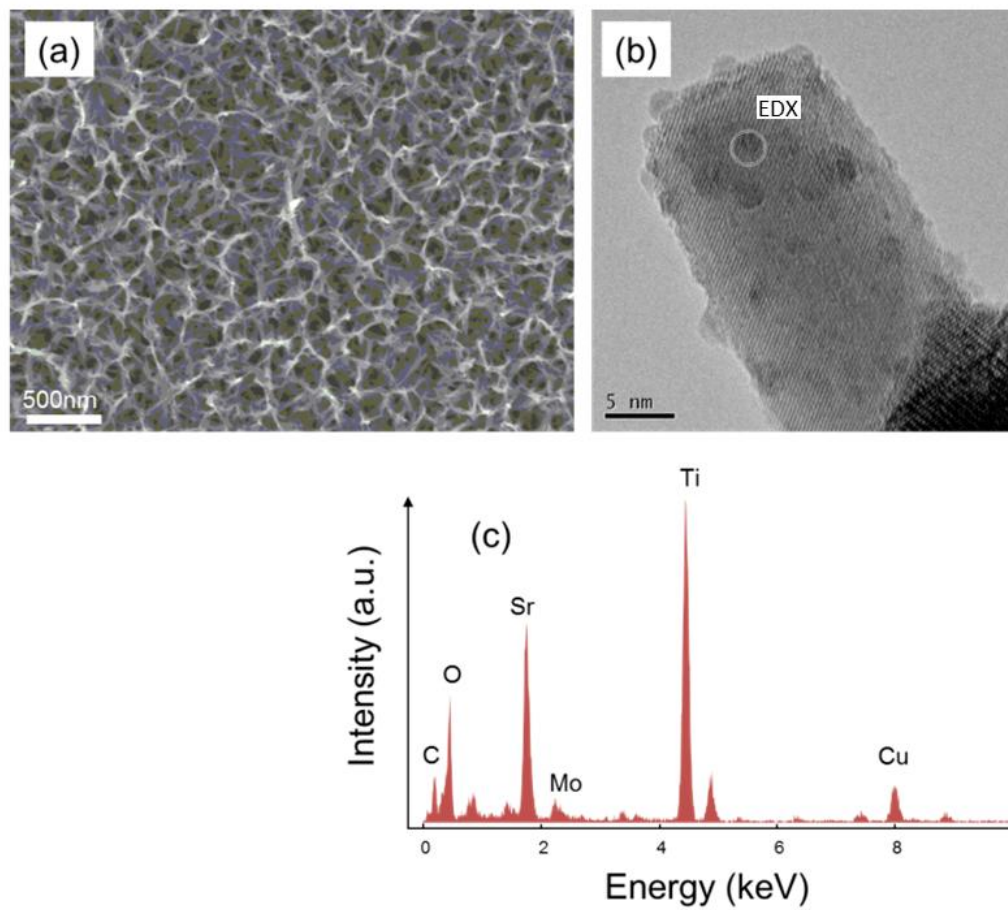
[Insert Running title of <72 characters]

Figure 1



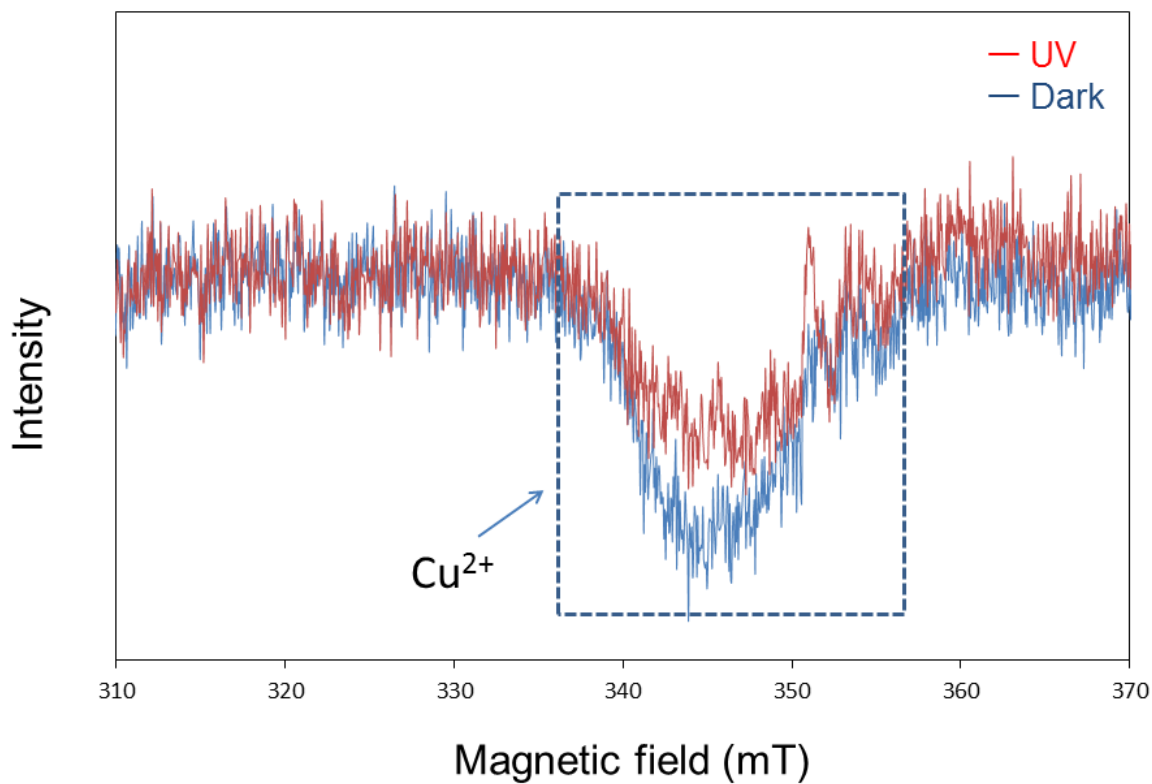
[Insert Running title of <72 characters]

Figure 2



[Insert Running title of <72 characters]

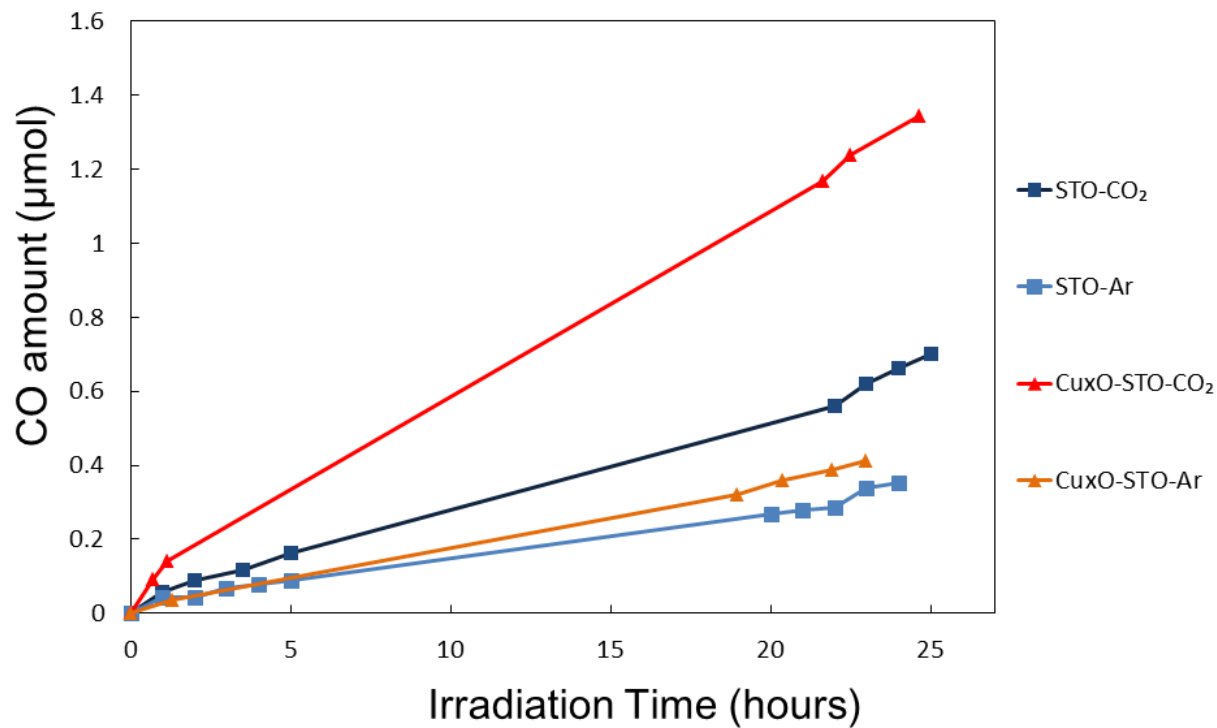
Figure 3



ACCEPTED

[Insert Running title of <72 characters]

Figure 4



ACCEPTED

[Insert Running title of <72 characters]

Figure 5

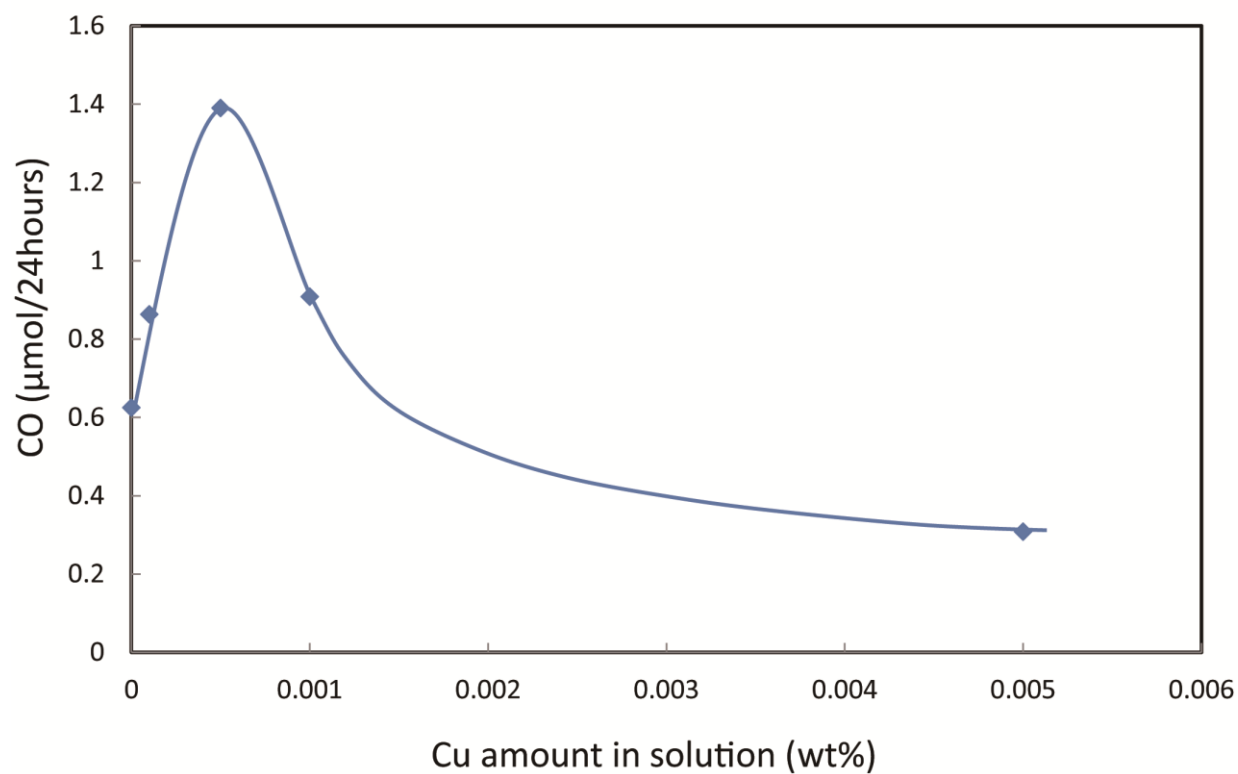
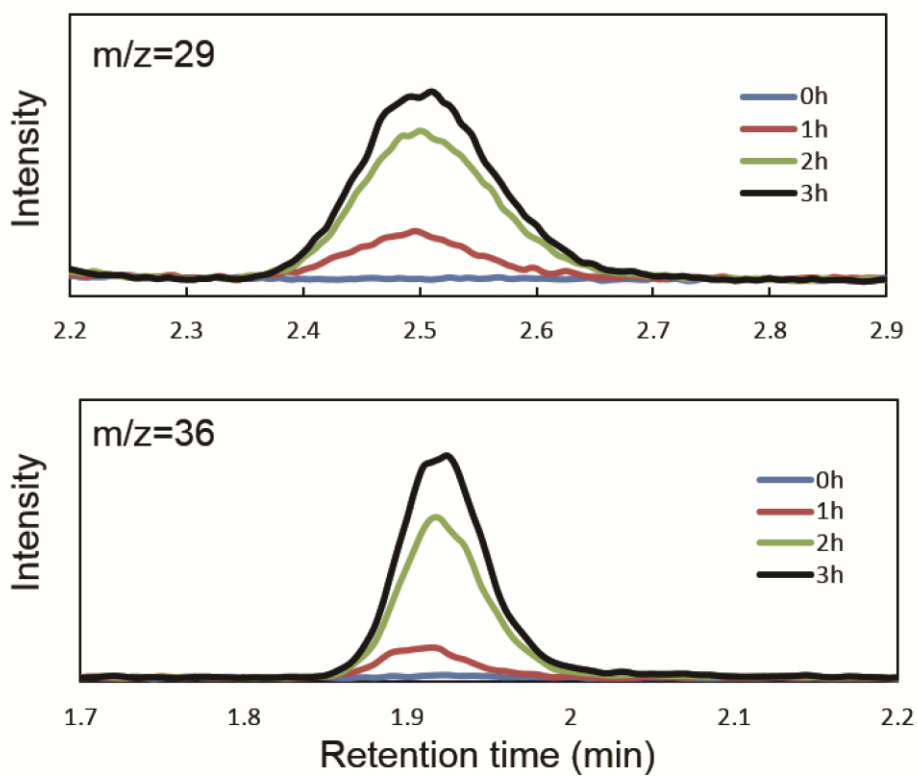


Figure 6



[Insert Running title of <72 characters]

Graphical abstract



[Insert Running title of <72 characters]

Highlight

- CO₂ photoreduction was achieved by the Cu_xO-cocatalysts loaded STO nanorod thin film.
- Cu_xO-cocatalysts were loaded by using a simple and economical impregnation method.
- Photocatalytic reaction mechanism was discussed by using electron spin resonance and isotope labeling analysis.

[Insert Running title of <72 characters]